

Vortex pairs in charged fluids

G. N. Stratopoulos* and T. N. Tomaras†

Department of Physics and Institute of Plasma Physics, University of Crete and Research Center of Crete, P.O. Box 2208, 710 03 Heraklion, Crete, Greece

(Received 9 February 1996; revised manuscript received 8 July 1996)

The motion of a vortex-(anti)vortex pair is studied numerically in the framework of a dynamical Ginzburg-Landau model, relevant to the description of a superconductor or of an idealized bosonic plasma. It is shown that up to a fine “cyclotron” internal motion, also studied in detail, two vortices that are brought together rotate around each other, while a vortex and an antivortex move in formation parallel to each other. The velocities of the vortices in both cases are measured to be in remarkable agreement with recent theoretical predictions, down to intervortex distances as small as their characteristic diameter. [S0163-1829(96)05541-5]

I. INTRODUCTION

The dynamics of flux vortices in ordinary¹ as well as high- T_C superconducting films² under the influence of a variety of external probes and for a wide range of temperatures has been an area of vigorous experimental and theoretical research during the past few decades. Their pinning by the impurities of the lattice, the role of their motion in energy dissipation, their contribution to the thermodynamic properties of a superconductor, and the statistical mechanics of a vortex lattice or of a vortex glass have received considerable attention.

However, due to both experimental and theoretical difficulties, no consensus on the equation of motion of an isolated vortex has been reached to date.³ Correspondingly, issues related to the existence and interpretation of the Magnus force on a vortex⁴ or to the origin of the so-called “opposite sign Hall effect” reported in all types of superconducting materials,⁵ as they are cooled below their critical temperature, have not yet been clarified.⁶ Experimentally, it is hard to isolate and directly observe the motion of a particular vortex in a superconducting film.⁷ So their dynamics is decided by an indirect interpretation of the measurements. The model that has often been used in the analysis of the experiments in the case of the superconductor is the effective model derived from the fundamental theory by Schmid⁸ or some of its subsequent variations and extensions.⁹ The equations get very involved and the analytical treatment not particularly transparent.⁶ In addition, the theoretical uncertainty over the proper incorporation of dissipation or over the precise role of “dirt” and impurities allows for little confidence in the details about vortex motion in fully realistic systems. Nevertheless, the overriding suggestion of all experiments is that vortex dynamics is in many ways contrary to intuition. The overall picture is reminiscent of the one that arises in the dynamics of analogous solitons (the magnetic bubbles) of the experimentally much simpler thin ferromagnetic films.¹⁰ Here, we were able to derive from first principles the equation of motion of the magnetic bubbles,¹¹ the semiempirical golden rule of bubble dynamics, as it has been called in the literature. In fact it became clear that the resulting “Hall motion” is a generic characteristic of soliton dynamics in systems with nontrivial topology and spontaneously broken

Galilean invariance, due for instance to the presence of a crystal lattice, properties shared by the superconductor.

Encouraged by this success, we proposed¹² as a modest first step to ignore finite-temperature and impurity effects and study the physics of flux vortices within the framework of a phenomenological effective field theoretic model,¹³ which in the terminology of Refs. 8 and 6 should describe the large friction limit of a pure superconductor at zero temperature. On the other hand, the model may also be thought of as the natural coupling to electromagnetism of the complex bosonic field of the Gross-Pitaevskii model for the superfluid, and as such it describes the dynamics of a charged bosonic plasma with the positive ions assumed infinitely heavy and frozen to form a homogeneous background. In a slightly formal jargon, the model considered is the most general one consistent with gauge symmetry and with a fixed homogeneous background which breaks Galilean invariance. More recent attempts towards a formal derivation of the effective action for the superconductor¹⁴ are quite encouraging for the physical relevance of the model at hand.

It was argued on general grounds that the model should support the existence of absolutely stable flux vortices¹² with finite energy per unit length, similar in nature to the previously known Abrikosov vortices¹⁵ of the static Ginzburg-Landau theory. The solutions were found numerically and their static properties as well as the properties of pairs of them, including their interaction potential, were studied in detail.¹⁶ They carry zero total electric charge, but have nonvanishing charge density and electric field and thus differ significantly from the ones studied before.

The equation of motion of the *guiding center* of the vortex under the influence of any external force was then derived,^{12,16} without any further assumption or approximation. For external forces weak relative to the characteristic scales of the system the guiding center is expected to describe accurately the position of the vortex. The precise quantitative condition though on the magnitude of the external force not to wildly deform the soliton and to guarantee a given accuracy is beyond our present analytical capabilities. Therefore, to clarify these issues, which is the main purpose of the present work, one has to rely on a numerical treatment of the equations. As a first step, in this paper we consider a vortex pair and a vortex-antivortex system in order to study

the motion of the vortex under the influence of the force due to another nearby (anti)vortex.

The paper is organized as follows: Sec. II contains a general introduction to the model as well as the study of the spectrum of small fluctuations around the vacuum. Its relevance to the physics of a superconductor is also commented upon. A brief review of the theoretical analysis of vortex dynamics is given for completeness in Sec. III. The notion of the guiding center is presented here together with the main predictions about the motion of the vortices in a vortex pair or in a vortex-antivortex system. The field equations of motion are subsequently solved numerically for a large variety of initial configurations and parameter values, and the results are presented in detail in Sec. IV. A remarkable agreement was established of the mean motion of each vortex with the theoretical formulas even when the solitons overlap considerably. Furthermore, regular patterns were observed in the vortex trajectories. They are reminiscent of the cyclotron motion of an electron pair in a perpendicular magnetic field and are also studied in detail.

II. MODEL: GENERAL PROPERTIES

The model describes the dynamics of a nonrelativistic charged scalar field Ψ , minimally coupled to the electromagnetic potential (A_0, A_i) . The Lagrangian density is

$$\mathcal{L} = \frac{i\gamma}{2}[\Psi^* \mathcal{D}_t \Psi - \text{c.c.}] + \gamma q \Psi_0^2 A_0 - \frac{\gamma^2}{2m} |\mathcal{D}_i \Psi|^2 + \frac{1}{8\pi} (\epsilon \mathbf{E}^2 - \mathbf{B}^2) - V(|\Psi|). \quad (1)$$

The magnetic and the electric fields are, respectively, $\mathbf{B} = \nabla \times \mathbf{A}$ and $E_i = (-1/c) \partial_t A_i - \partial_i A_0$, while $\mathcal{D}_i \Psi = (\partial_i + iqA_0) \Psi$, $\mathcal{D}_i \Psi = [\partial_i - i(q/c)A_i] \Psi$. A quartic phenomenological potential $V(|\Psi|) = \frac{1}{8g} (\Psi \Psi^* - \Psi_0^2)^2$ may or may not be present, depending on the physical system of interest. γ , m , ϵ , g , and q are parameters, c is the speed of light, and the spatial indices i and j range from 1 to the dimensionality of space. For simplicity we did not include an arbitrary parameter in front of the term \mathbf{B}^2 . Up to this inessential for our purposes restriction, the model is the most general theory possessing translational, rotational, and gauge symmetry. To make the model consistent we have included a background (positive-ion) charge density $q\Psi_0^2$ to neutralize the system. We work in the limit where ions are very heavy and the background is taken nondynamical.

We switch to dimensionless fields and coordinates by the rescalings

$$x_i \rightarrow \frac{\sqrt{mc}}{\sqrt{4\pi\Psi_0 q \gamma}} \tilde{x}_i, \quad t \rightarrow \frac{m^2 c^2}{4\pi\Psi_0^2 q^2 \gamma^3} \tilde{t},$$

$$\Psi \rightarrow \Psi_0 \tilde{\Psi}, \quad A_0 \rightarrow \frac{4\pi\Psi_0^2 q \gamma^3}{m^2 c^2} \tilde{A}_0, \quad A_i \rightarrow \frac{\sqrt{4\pi\Psi_0} \gamma}{\sqrt{m}} \tilde{A}_i, \quad (2)$$

and write the Lagrangian in the form

$$\mathcal{L} = \frac{1}{2} [\tilde{\Psi}^* (i\tilde{\partial}_t - \tilde{A}_0) \tilde{\Psi} + \text{c.c.}] + \tilde{A}_0 - \frac{1}{2} |\tilde{D}_i \tilde{\Psi}|^2 + \frac{1}{2} \left(\frac{1}{\beta} \tilde{\mathbf{E}}^2 - \tilde{\mathbf{B}}^2 \right) - \frac{1}{8} \kappa^2 (\tilde{\Psi} \tilde{\Psi}^* - 1)^2, \quad (3)$$

with $\tilde{\mathbf{B}} = \nabla \times \tilde{\mathbf{A}}$, $\tilde{E}_i = -\tilde{\partial}_t \tilde{A}_i - \tilde{\partial}_i \tilde{A}_0$, and $\tilde{D}_i = \tilde{\partial}_i - i\tilde{A}_i$. The two remaining parameters, the quartic self-coupling κ^2 and the coupling β (notice that we have changed the name λ we used in Ref. 16 for the second parameter to β , in order to avoid confusion with the standard notation of the penetration depth of a superconductor) of the scalar field to the electrostatic potential, are defined by

$$\kappa^2 = \frac{gm^2 c^2}{4\pi q^2 \gamma^4}, \quad \beta = \frac{m^3 c^4}{4\pi \epsilon q^2 \gamma^4 \Psi_0^2}. \quad (4)$$

With the identification of the field Ψ as the condensate wave function of the Cooper pairs, and correspondingly with $\gamma = \hbar$, $m = 2m_e$, and $q = 2e/\hbar$, Eq. (1) becomes a rather realistic phenomenological model of a superconductor. It offers a natural explanation of the Meissner and the Josephson effects, and it predicts the correct value of the quantum $\phi_0 = 2.09 \times 10^{-7}$ G cm² of the vortex magnetic flux.¹³ As follows from Eqs. (2), the units of length and time depend only on the parameter Ψ_0 which is fixed by the condensate number density. For values of the latter equal to a few percent of the valence electron density, the characteristic length falls in the range 100–1000 Å, while the time unit is 10^{-10} – 10^{-8} sec. In these units the penetration depth λ is equal to 1 [see Eq. (15) below]. The coherence length ξ on the other hand depends on both parameters κ and β . For κ much smaller than 1 it varies as $\beta^{-1/4}$, while for β much smaller than 1 its dependence is κ^{-1} .¹⁷ Thus, one way to fit a realistic ratio $\xi/\lambda = 0.25$ of a type-II superconductor is to take κ small and $\beta \approx 4^4$. As we will demonstrate, though in the sequel, the main features of vortex motion are robust and independent of the particular parameter values.

The action S , the integral of \mathcal{L} over space and time, is invariant under the gauge transformation (to simplify notation all tilde shall be dropped from now on)

$$\Psi' = \exp[i\Lambda(\mathbf{x}, t)] \Psi,$$

$$A_i' = A_i + \partial_i \Lambda, \quad (5)$$

$$A_0' = A_0 - \partial_t \Lambda,$$

for arbitrary function $\Lambda(\mathbf{x}, t)$, and its extremization with respect to A_0 leads to the Gauss constraint

$$\frac{1}{\beta} \partial_i E_i = \Psi \Psi^* - 1. \quad (6)$$

We shall only be interested in configurations with vanishing total electric charge. The equations of motion derived by varying S (under this constraint) with respect to Ψ^* and A_i read

$$i\dot{\Psi} = -\frac{1}{2}\mathbf{D}^2\Psi + A_0\Psi + \frac{1}{4}\kappa^2(\Psi^*\Psi - 1)\Psi,$$

$$\frac{1}{\beta}\dot{\mathbf{E}} = \nabla \times \mathbf{B} - \mathbf{J}, \quad (7)$$

with the current $\mathbf{J} = [\Psi^*\mathbf{D}\Psi - \text{c.c.}]/2i$. The energy W of an arbitrary configuration of the system is the spatial integral of the energy density w , which is the sum $w = w_d + w_b + w_e + w_v$ of the four positive definite terms

$$w_d = \frac{1}{2}|D_i\Psi|^2, \quad w_b = \frac{1}{2}\mathbf{B}^2, \quad w_e = \frac{1}{2\beta}\mathbf{E}^2,$$

$$w_v = \frac{1}{8}\kappa^2(\Psi\Psi^* - 1)^2. \quad (8)$$

The vacuum

Equations (6) and (7) admit the one-parameter family of equivalent vacuum solutions

$$\Psi = e^{i\alpha}, \quad A_i = 0, \quad A_0 = 0, \quad (9)$$

parametrized by the constant angular parameter α .

To study the spectrum of small fluctuations around the vacuum solution we choose the one with $\alpha = 0$ and the Coulomb condition $\nabla \cdot \mathbf{A} = 0$ to remove the gauge arbitrariness of the model. We then parametrize the generic deviation of Ψ from its vacuum value $\Psi = 1$ by

$$\Psi = (1 + \Phi)e^{i\Theta}. \quad (10)$$

For the discussion of small fluctuations the magnitudes of Φ , Θ , A_0 , and A_1 will all be taken much smaller than 1. Keeping only up to quadratic terms in these small fields, the Lagrangian becomes

$$\mathcal{L} = -\partial_t\Theta(1 + 2\Phi) - 2\Phi A_0 - \frac{1}{2}(\partial_i\Theta^2 + \partial_i\Phi^2 + A_i^2)$$

$$+ \frac{1}{2\beta}(\partial_i A_0^2 + \partial_i A_i^2) - \frac{1}{2}\mathbf{B}^2 - \frac{1}{2}\kappa^2\Phi^2 \quad (11)$$

and the equations of motion read

$$\partial_t\Phi + \partial_i^2\Theta = 0, \quad (12)$$

$$\partial_t\Theta = \frac{1}{2}\partial_i^2\Phi - A_0 - \frac{1}{2}\kappa^2\Phi, \quad (13)$$

$$\frac{1}{\beta}\partial_i^2 A_0 + 2\Phi = 0, \quad (14)$$

$$\frac{1}{\beta}\partial_i^2 A_i = \partial_k^2 A_i - A_i. \quad (15)$$

The field A_i decouples at this level. Acting with the time derivative on Eq. (12), with the Laplacian on Eq. (13) and using Eq. (14), one obtains the following equation of motion of Φ :

$$\partial_t^2\Phi = \frac{1}{4}\kappa^2\partial_i^2\Phi - \beta\Phi - \frac{1}{4}\partial_i^4\Phi. \quad (16)$$

The plane waves $A_i = A_i^0 e^{-i(\omega_A t - \mathbf{k} \cdot \mathbf{x})}$ and $\Phi = \Phi^0 e^{-i(\omega_\Phi t - \mathbf{k} \cdot \mathbf{x})}$, obeying the dispersion relations

$$\omega_\Phi^2 = \beta + \frac{1}{4}\kappa^2|\mathbf{k}|^2 + \frac{1}{4}|\mathbf{k}|^4, \quad (17)$$

$$\omega_A^2 = \beta(1 + |\mathbf{k}|^2), \quad (18)$$

form a complete set of solutions of the equations of motion of Φ and A_i above. Notice that both spectra $\omega_\Phi(\mathbf{k})$ and $\omega_A(\mathbf{k})$ have an energy gap $G = \sqrt{\beta}$. Finally, the solutions for Θ and A_0 are obtained by solving Eqs. (12) and (14), respectively.

III. VORTEX DYNAMICS

The model under study, with or without the potential term $V(|\Psi|)$ present, supports the existence of flux vortex solutions. They are infinitely long, localized in the transverse direction, smooth, cylindrically symmetric, z -independent configurations with finite energy per unit length, whose static properties, together with the properties of pairs of them, have been studied in detail.¹⁶ We wish to study their dynamics numerically and to verify the approximate analytical predictions about their motion,¹² reviewed briefly in the present section. We will ignore the z -dependent excitations of the string and consequently the formalism reduces to purely 2 + 1 dimensional. Spatial indices will from now on take the values 1 and 2, while the magnetic field will only have its third component nonvanishing and will be simply denoted by B . Correspondingly, we will be thinking of the vortices as finite-energy ‘‘particlelike’’ localized objects in two spatial dimensions. Any finite-energy configuration is characterized by an absolutely conserved integer number N , which counts the number of times the phase of the scalar field at spatial infinity, a function of the polar angle θ , winds around the circle of vacua, Eq. (9), as θ varies from zero to 2π . It is evaluated for the given configuration by integrating over space a topological density $\tau(\mathbf{x})$. Among the various possibilities the most useful form of τ is, for our purposes, the manifestly gauge invariant expression

$$\tau = \frac{1}{2\pi i}[\epsilon_{kl}(D_k\Psi)^*(D_l\Psi) - iB(\Psi^*\Psi - 1)]. \quad (19)$$

As will be shown immediately, this quantity appears in the formulas for the conserved momentum and angular momentum of the theory.

Indeed, it was pointed out in Ref. 12 that the naive Noether expressions for the linear and the angular momentum of the model are ambiguous for any configuration with nonzero topological charge, and that the correct formulas for these quantities are

$$P_k = \epsilon_{ki} \int d^2x \left(2\pi x_i \tau + \frac{1}{\beta} E_i B \right) \quad (20)$$

and

$$l = - \int d^2x \left(\pi \mathbf{x}^2 \tau + \frac{1}{\beta} \mathbf{x} \cdot \mathbf{E} B \right), \quad (21)$$

respectively. They differ from the naive expressions by surface terms, which are important in topologically nontrivial

sectors. The presence of the first and the second moments of the topological density τ in the above formulas inherits them with an entirely different physical meaning. Let us consider the momentum. Rotate it by 90° and divide by the constant $2\pi N$ to obtain the new conserved quantity

$$R_i \equiv -\frac{1}{2\pi N} \epsilon_{ij} P_j. \quad (22)$$

The value of \mathbf{R} for an isolated axially symmetric vortex solution is exactly the center of the vortex, and a rigid displacement by \mathbf{c} of any given configuration as a whole changes \mathbf{R} by \mathbf{c} . Thus, the natural interpretation of \mathbf{R} is the ‘‘mean position’’ of a generic localized configuration and this justifies the name *guiding center* for it. Similarly, the first term of the angular momentum is a measure of the size of the localized configuration and not of its rotational motion.

Finally, one should mention the fact that the two components of the momentum, the generators of translations in the x and the y directions, do not commute. Instead, their Poisson brackets are

$$\{P_1, P_2\} = 2\pi N, \quad (23)$$

a property suggesting a deep algebraic similarity of the model under study to a system of electric charges moving in a plane and in the presence of a perpendicular magnetic field.¹¹ Up to a multiplicative constant, the topological charge plays the role of the external magnetic field of the analogue model.

In the absence of external forces \mathbf{P} is constant and so is \mathbf{R} . Thus, a free localized vortex whose mean position is given by \mathbf{R} will be spontaneously pinned at its initial position. No free translational motion of a vortex is possible. Under the influence of an external force \mathbf{F} , the momentum evolves according to Newton’s law $dP_k/dt = F_k$ and this translates into the following equation of motion of the vortex:

$$\frac{d}{dt} R_k = -\frac{1}{2\pi N} \epsilon_{kl} F_l; \quad (24)$$

i.e., the vortex moves with speed $|\mathbf{F}|/2\pi|N|$ and at $\pm 90^\circ$ relative to the force for positive and negative N , respectively. We see that the vortices exhibit the Hall behavior known from the analog electric charge system mentioned above. This is how the analogy of the canonical structures of the two systems is reflected in the dynamics.

Based on Eq. (24), one may immediately conclude that the vortices of a vortex pair will rotate around each other. A rough theoretical estimate of the corresponding angular velocity Ω is easily obtained, especially when both vortices carry the same number N of flux quanta. Define for each one of the two vortices its approximate guiding center by Eqs. (22) and (20) with the integral taken over the corresponding half-plane. For localized vortices separated by a distance d , large compared to their characteristic size, this is a reasonable definition of their positions. Let us further assume that each vortex behaves more or less like a rigid body living in a potential equal to the vortex-vortex interaction energy $U_{vv}(d)$. Then, the magnitude of Ω is given by

$$\Omega(d) = \frac{1}{\pi|N|d} |U'_{vv}(d)| \quad (25)$$

and its direction is counterclockwise (clockwise) for $N\mathbf{\Delta} \cdot \mathbf{F}$ positive (negative), respectively. The vector $\mathbf{\Delta}$ joins the center of the system to the approximate position of any one of the two vortices, while \mathbf{F} denotes the force acting on it.

In the same spirit, a vortex-antivortex pair with $N(-N)$ flux units, respectively, is expected to move in formation in a direction perpendicular to the line connecting them, and with a speed given by

$$V(d) = \frac{1}{2\pi|N|} |U'_{vv}(d)|. \quad (26)$$

The direction of their motion coincides with that of $\mathbf{r} \times \hat{\mathbf{z}}$, where $\mathbf{r} \equiv \mathbf{R}_+ - \mathbf{R}_-$ the vector joining the negative to the positive-flux vortex, and $\hat{\mathbf{z}}$ the unit vector out of the plane. Incidentally, one may check that, like in the relativistic Abelian-Higgs model,¹⁸ the vortex and the antivortex attract at all distances, a fact used above in the determination of the direction of motion of the pair.

Clearly, formulas (25) and (26) should not *a priori* be trusted for very small separations of the two solitons. Although for d much larger than their characteristic size the hypotheses behind their derivation are physically sound, smaller d ’s make such approximations questionable. It will be shown though in the next section, through a direct quantitative comparison of these formulas with our numerical results, that Eqs. (25) and (26) are reliable and describe quite accurately the vortex-(anti)vortex motion even at distances as small as their characteristic diameter.

IV. NUMERICAL RESULTS

A. Discretization

We now turn to the numerical treatment of the motion of a pair of vortices and of a vortex-antivortex system due to their mutual interaction. We choose to discretize the system in a way that preserves as much of the symmetry of the continuous theory as possible. In particular, as explained in the Appendix, it is convenient to preserve the gauge invariance of the model. Otherwise one has difficulty in imposing Gauss’ local constraint, and this leads to integration instabilities. But then naive discretization of the model is not appropriate and one has instead to use techniques developed in the study of lattice gauge theories.¹⁹

Space is replaced by a two-dimensional square lattice with lattice spacing a . The scalar field is replaced by the variables $\Psi_{i,j}$, all functions of time, which live on the vertices of the lattice. Similarly, the spatial components of the gauge field are represented by $A_{i,j}^1$ and $A_{i,j}^2$ and live on the corresponding oriented link connecting (i,j) to $(i+1,j)$ and to $(i,j+1)$, respectively. At this stage time is left continuous and the electrostatic potential $A_{i,j}^0$ lives on the vertices of the grid.

The lattice version of the covariant derivative is

$$D_k \Psi_{i,j} = \frac{1}{a} (U_{i,j}^k \Psi_{(i,j)+\hat{k}} - \Psi_{i,j})$$

where

$$U_{i,j}^k = \exp(-iaA_{i,j}^k), \quad (27)$$

and the lattice action takes the form

$$S = \int dt a^2 \sum_{i,j} \left\{ \frac{1}{2} [\Psi_{i,j}^* (i\partial_t - A_{i,j}^0) \Psi_{i,j} + \text{c.c.}] \right. \\ \left. + A_{i,j}^0 - \frac{1}{2} |D_k \Psi_{i,j}|^2 + \frac{1}{2\beta} \mathbf{E}_{i,j}^2 - \frac{1}{8} \kappa^2 (\Psi_{i,j}^* \Psi_{i,j} - 1)^2 \right. \\ \left. - \frac{1}{2a^4} [1 - \cos[a(A_{i,j}^1 + A_{i,j+1}^2 - A_{i+1,j}^1 - A_{i,j}^2)]] \right\}, \quad (28)$$

where $E_{i,j}^k = -\partial_t A_{i,j}^k - (1/a)(A_{(i,j)+\hat{k}}^0 - A_{(i,j)}^0)$. In the $a \rightarrow 0$ limit the last term of Eq. (28) becomes the B^2 term of the continuous model.

The action (28) is indeed invariant under the discrete version of the gauge transformation (5):

$$\Psi_{i,j} \rightarrow \exp(i\Lambda_{i,j}) \Psi_{i,j}, \\ A_{i,j}^k \rightarrow A_{i,j}^k + \Lambda_{(i,j)+\hat{k}} - \Lambda_{i,j}, \quad (29) \\ A_{i,j}^0 \rightarrow A_{i,j}^0 + \partial_t \Lambda_{i,j}.$$

Correspondingly, the system obeys the discretized form of Gauss' law:

$$\frac{1}{a} \sum_{k=1,2} (E_{(i,j)+\hat{k}}^k - E_{i,j}^k) = \beta (\Psi_{i,j}^* \Psi_{i,j} - 1), \quad (30)$$

where \hat{k} is the unit lattice step in the spatial direction k . Variation of the lattice action (28) with respect to $\Psi_{i,j}^*$ and $A_{i,j}^k$ leads to the equations of motion

$$i\dot{\Psi} = \frac{1}{2a} \sum_{k=1,2} \{ U_{(i,j)-\hat{k}}^{k*} (D_k \Psi_{(i,j)-\hat{k}}) - (D_k \Psi_{(i,j)}) \} \\ + \frac{1}{4} \kappa^2 (\Psi_{i,j}^* \Psi_{i,j} - 1) \Psi_{i,j}, \\ \frac{1}{\beta} \dot{E}_{i,j}^k = \frac{i}{2a} [U_{i,j}^k \Psi_{i,j+\hat{k}} \Psi_{i,j}^* - U_{i,j}^{k*} \Psi_{i,j+\hat{k}}^* \Psi_{i,j}^*] \\ + \frac{1}{2a^3} \sum_{l \neq k} \{ \sin[a(A_{i,j}^k + A_{i,j+\hat{k}}^l - A_{i,j+\hat{l}}^k - A_{i,j}^l)] \\ - \sin[a(A_{i,j-\hat{l}}^k + A_{i,j+\hat{k}-\hat{l}}^l - A_{i,j}^k - A_{i,j-\hat{l}}^l)] \}. \quad (31)$$

Equations (31) will be integrated numerically, in order to follow the time evolution of any set of initial data obeying the local constraint (30). Notice that no A_0 appears in the equations above. They are written in the $A_0 = 0$ gauge, which simplifies considerably the equations of motion and makes the numerical task more tractable. We leave for the Appendix the details about the lattice size, the time discretization, and the integration algorithm used, and proceed with the presentation of our results.

B. Vortex pair

Let us consider two vortices with N units of magnetic flux each, formed initially at a distance d from one another. In terms of the fields Ψ and A_i it is most convenient to take for the initial configuration the ‘‘product ansatz’’ of the corresponding two axially symmetric vortex solutions¹⁶

$$\Psi(\mathbf{x}) = \Psi^{(N)}\left(\left|\mathbf{x} - \frac{\mathbf{d}}{2}\right|\right) \Psi^{(N)}\left(\left|\mathbf{x} + \frac{\mathbf{d}}{2}\right|\right), \quad (32)$$

$$\mathbf{A}(\mathbf{x}) = \mathbf{A}^{(N)}\left(\left|\mathbf{x} - \frac{\mathbf{d}}{2}\right|\right) + \mathbf{A}^{(N)}\left(\left|\mathbf{x} + \frac{\mathbf{d}}{2}\right|\right). \quad (33)$$

The field A_0 is consistently set to zero, while the solution of Gauss' constraint for the given Ψ configuration provides us with the initial data for the electric field $-\partial_t A_i(\mathbf{x}, t=0)$, necessary for the integration of the equations of motion.

Although for large separations this configuration is somewhat special, being close to the minimum of the energy under the constraint of two zeros in the scalar field, for smaller d it imitates reasonably well the rather random production of the vortices in a realistic situation. (In fact, the axial symmetry of the ‘‘individual vortices’’ was relaxed in several runs. No deviations from the picture presented below were observed.) Thus, the initial configuration consists essentially of two lumps of energy and topological charge, concentrated around two local maxima at a distance d from one another. Strictly speaking, there is no unique definition of a vortex position in a generic multivortex configuration. The positions

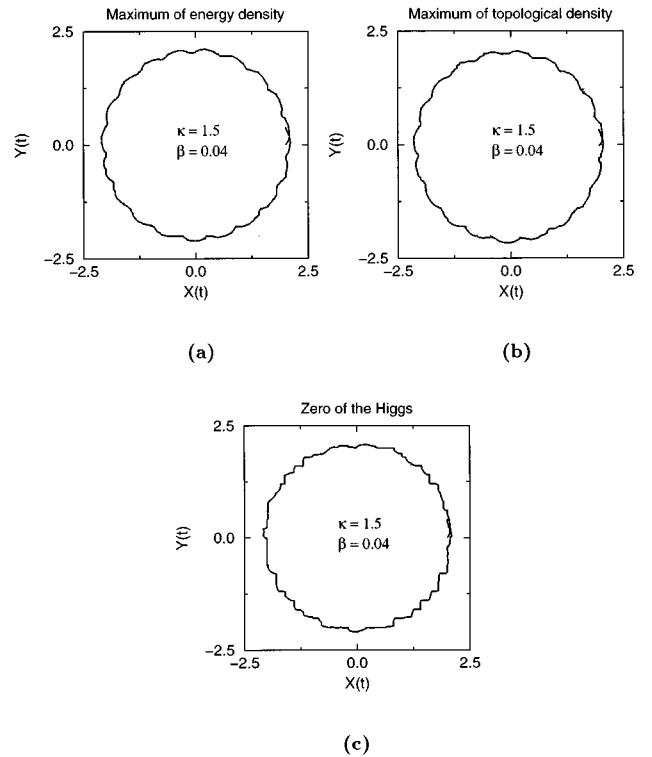


FIG. 1. The trajectory of one vortex in the pair as determined by the location of the maximum of the energy density, of the maximum of the topological density, and of the zero of the scalar field Ψ . Time duration $t=800$.

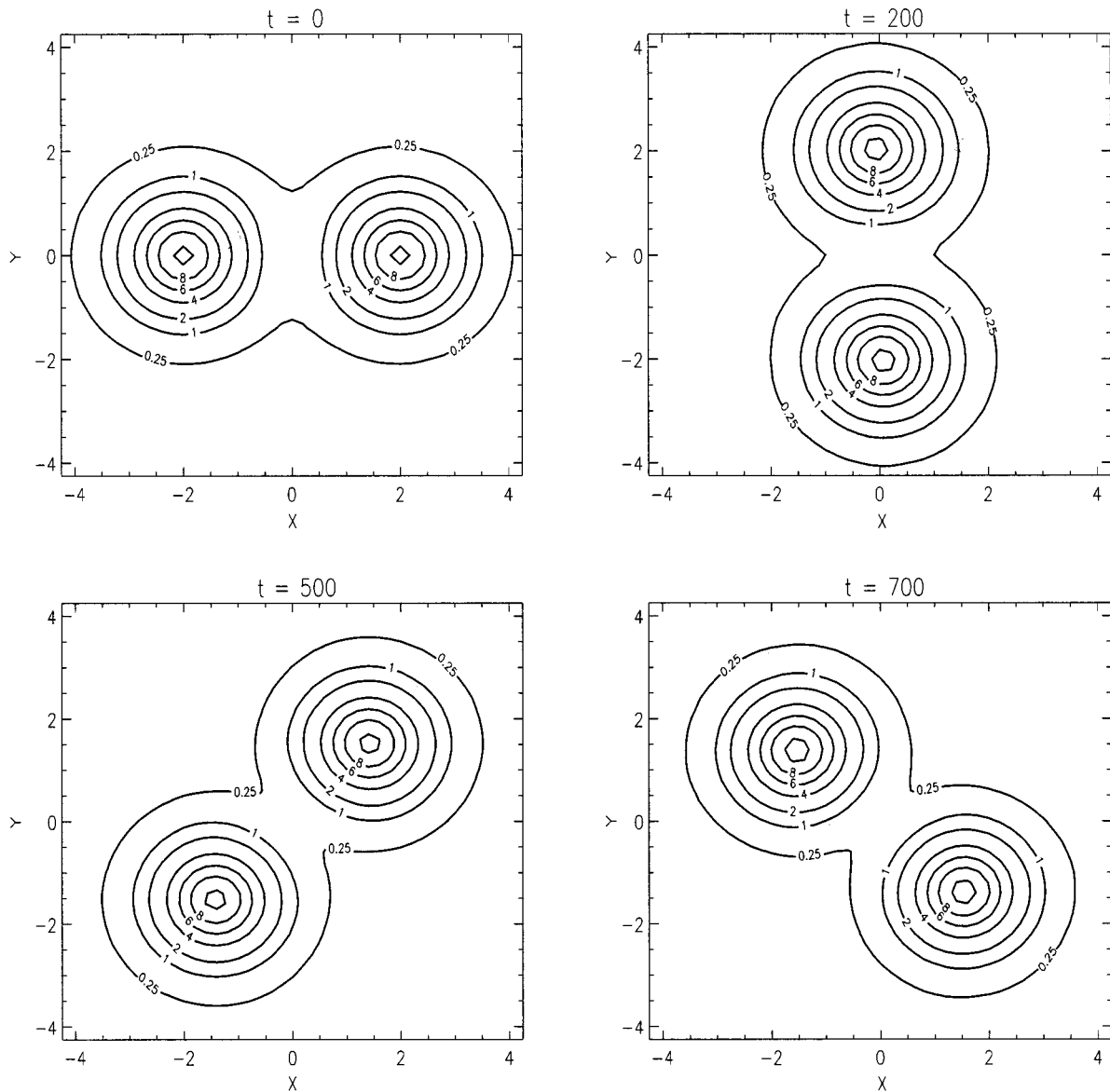


FIG. 2. Four snapshots of the energy density contours during the motion of the vortex pair. The values of the energy density on the contours, the time and the distances on the X and Y axes are given in the units defined by Eq. (2).

of the individual vortices are defined only approximately, either as the positions of the zeros of the scalar field, or as the positions of the local maxima of the energy density or of the topological density, or finally as the approximate guiding centers discussed in the previous section. All these are reasonable definitions and their differences become less and less significant as one increases the vortex separation. Having specified the initial configuration one is ready to proceed with the numerical study of its time evolution.

We take for the parameters the values $\kappa=1.5$ and $\beta=0.04$ and consider first the case of two minimal $N=1$ vortices. Figures 1 and 2 show the results of the numerical integration with the two vortices placed initially at $(-2.0, 0)$ and $(+2.0, 0)$, respectively. At this distance the vortices already interact significantly, while retaining their individuality. In Fig. 1 the trajectory of the second vortex is plotted. The first one follows the image of the above trajectory under reflection with respect to the origin. To avoid overlapping of the trajectories,

the run was interrupted after about 800 time units, when the vortices had each completed a full rotation around the origin. The picture that emerges is identical to the one obtained in the study of the motion of a pair of electrons in the plane and in the presence of a perpendicular magnetic field.^{17,20} Apart from an overall rotation around the origin, a finer periodic motion can be perceived in the trajectory of each vortex, shown in Fig. 1. Borrowing the terminology from the two-electron analog, we give the name “cyclotron” to this finer motion of the vortices and we will study it in detail later on.

The fact that the trajectories shown in Fig. 1 are so similar indicates that the vortices move like rigid bodies, without significant oscillatory activity in their interiors. This is demonstrated beyond any doubt also in Fig. 2, where we plot four snapshots of the energy density contours, corresponding to times $t=0$, $t=200$, $t=500$, and $t=700$, respectively. In agreement with our previous conclusion, the shape of the energy profile in each of the two lumps seems to remain

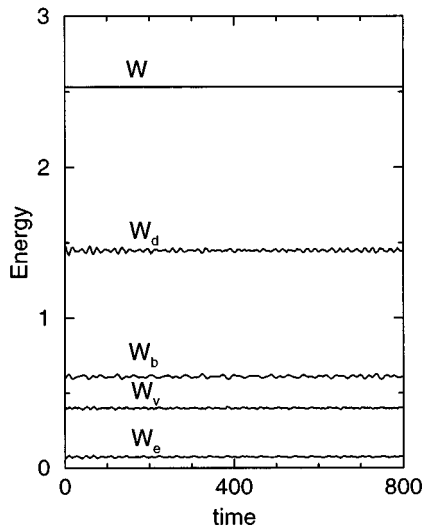


FIG. 3. The time dependence of the various components of the energy of the vortex pair and of the total energy W . Note the high accuracy in the conservation of the total energy of the system.

unchanged during the rotation. A more detailed examination though, including animation of successive snapshots, revealed a small oscillation in the sizes of the two energy lumps. They spread a little and shrink periodically with a period equal to that of the cyclotron motion.

An estimate of the accuracy of the results presented above is obtained by examining the precision of the validity of the conservation laws during the evolution. Thus we consider next the time dependence of the theoretically conserved quantities: energy, linear momentum, angular momentum, and topological charge, as well as the local constraint given by Gauss' law. After a complete period, the total deviation in Gauss' law (the sum over all points of the grid of the absolute values of the local deviations) was less than 10^{-6} . From the time evolution of the total energy W of the system, depicted in Fig. 3, one sees that it was conserved with an accuracy better than one part in 10^3 . In contrast to the vividly oscillating four components W_e , W_b , W_d , and W_v , also plotted in the same figure, the total energy is on the same scale a perfect straight line parallel to the time axis. The same is true for the total angular momentum l and its two gauge-invariant pieces l_1 and l_2 , all plotted in Fig. 4. Although the two individual terms undergo rather wild oscillations, their sum is conserved to within a few percent. The first term l_1 of the angular momentum (21) is $-\pi$ times the second moment of the topological density, a measure of the size of the vortex pair. Thus, the oscillatory nature of the cyclotron motion of the two vortices, shown in Fig. 1 above, is expected to induce a similar behavior in the time evolution of l_1 , while the conservation of the total angular momentum implies the same for l_2 , all with the same period. This is trivially verified by a comparison of Figs. 1 and 4. Note that a periodical pattern with the same period can also be detected in the energy plots after careful examination. It seems that this oscillatory behavior is a general feature of the system. We turn next to the total topological charge N , whose time evolution is plotted in Fig. 5. N starts at $t=0$ with the value 1.993, and up to a small fluctuation of less than one part in

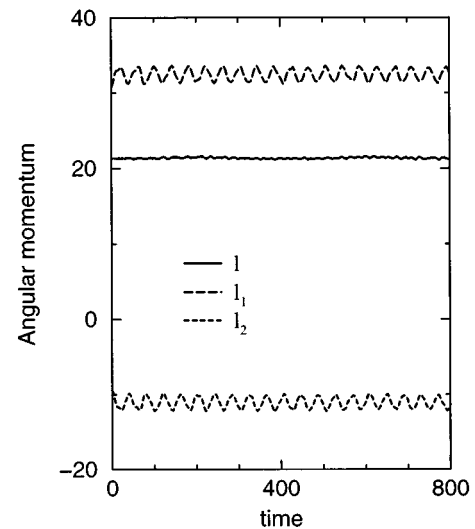


FIG. 4. The two pieces of the angular momentum and their sum. The conservation of the total angular momentum to within 2% is quite satisfactory.

10^3 it retains that value for the whole duration of the run. Its deviation from the continuum value $N=2$ is due to the spatial discretization of the system. Finally, the position of the guiding center of the system (or equivalently its total linear momentum) is considered. This is a conserved quantity, which, due to the symmetry of the starting configuration, initially coincides with the origin of the coordinate system. It was checked to be pinned there with impressive accuracy at all times.

Thus, the picture that arises clearly confirms the theoretical predictions discussed in the previous section. All the conserved quantities of the continuum are respected with high accuracy. Furthermore the system is characterized by periodic patterns manifested in the trajectory plots, one example of which is what we called "cyclotron motion." This whole qualitative picture is generic. It was verified in all our runs, for a large variety of initial configurations and for a wide range of parameter values.

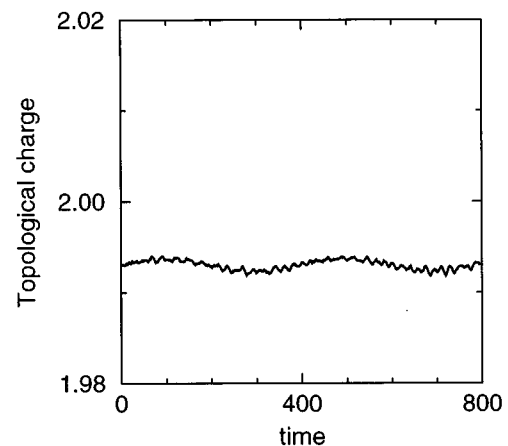


FIG. 5. The time evolution of the total topological charge of the vortex pair.

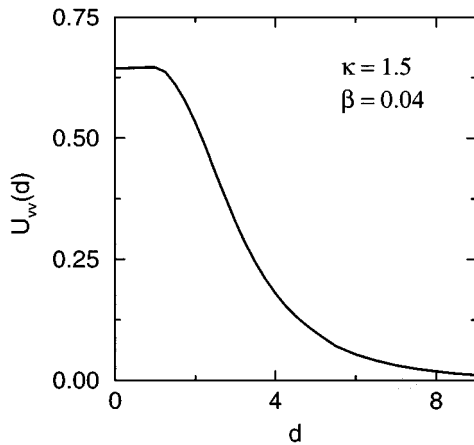


FIG. 6. The interaction energy of two $N=1$ vortices for $\kappa=1.5$ and $\beta=0.04$ as a function of their separation d .

We proceed next to the quantitative comparison of our numerical results with the rough theoretical prediction (25) of the angular velocity of the vortex rotation. For that one needs the interaction potential $U_{vv}(d)$ between the two vortices as a function of their distance. Define $U_{vv}(d) = E(d) - 2E_{N=1}$, with $E(d)$ the minimum of the energy in the $N=2$ sector with the constraint that the scalar field vanishes at two points, a distance d apart, and $E_{N=1}$ the energy of the single-vortex solution. The result for $\kappa=1.5$ and $\beta=0.04$ is plotted in Fig. 6. One sees that for the values of the parameters chosen above, $U_{vv}(d)$ is repulsive at all distances, falling to zero very quickly. With the interaction energy $U_{vv}(d)$ at hand one may calculate numerically its derivative and plot the theoretical prediction for the period of revolution derived from the right-hand side of Eq. (25). This is illustrated by the continuous curve in Fig. 7. One then simulates numerically the motion of the vortex pair for various initial separations and from the time it takes for them to cover a full circle around each other one determines the cor-

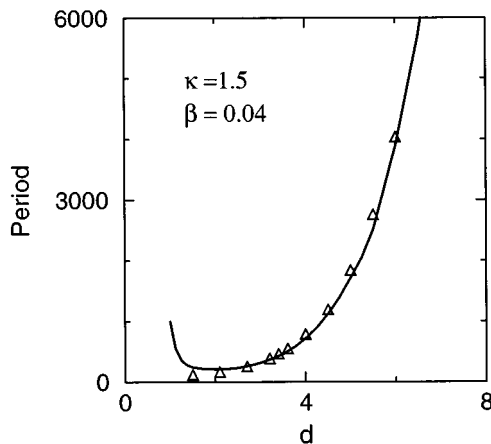


FIG. 7. The period of revolution of the vortices around each other as a function of their separation, computed from the theoretical formula using the slope of the curve of Fig. 6 (solid line) and from the numerical experiments (triangles).

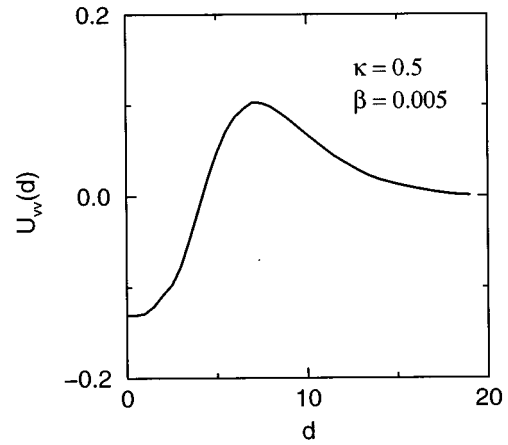


FIG. 8. The interaction potential of the two vortices for $\kappa=0.5$ and $\beta=0.005$. The potential is attractive for small distances and repulsive for $d > 7$.

responding period. The result is represented by the little triangles in Fig. 7. The agreement is quite remarkable, down to distances of the order of the vortex characteristic diameter, at which the two vortices overlap almost to the point of losing their individuality.

It was pointed out in Ref. 16 that in contrast to the vortex-antivortex which always attract each other,¹⁸ the interaction energy $U_{vv}(d)$ between two vortices is not in general a monotonically decreasing function of their distance. For instance, the potential $U_{vv}(d)$ for the model with $\kappa=0.5$ and $\beta=0.005$ shown in Fig. 8 increases up to a local maximum at $d=7$ and decreases beyond that. In agreement with Eq. (25) one then expects the two $N=1$ vortices to rotate counterclockwise when put at a distance greater than 7, and clockwise when the initial separation is smaller than 7. This is exactly what is observed for two vortices placed initially on the x axis, symmetrically with respect to the origin at a distance $d=8$ and $d=4.5$, respectively. The trajectories of the vortices initially on the right, as determined by the zero of the scalar field, are shown for both cases in Fig. 9. The absolute values of the corresponding angular velocities are also in agreement with Eq. (25). The rather vivid fluctuations in the details of the two interacting vortices is a general feature in small κ models.

Before we move on to the discussion of the vortex-antivortex system, and in order to improve one's intuition about the behavior of the vortex pair, we would like to push a bit further its qualitative analogy with the two-electron system. For that we will study and compare the details of their cyclotron motions. The simplicity of the electron system allows for a complete analytical treatment and for a detailed description of their trajectories. One finds^{17,20} that generically the corresponding guiding centers perform circular motion, while the orbits of the electrons themselves exhibit patterns similar to those of Fig. 1. Furthermore, it can be shown that for given initial conditions, the characteristic wavelength and width of their cycloid motions increase when one decreases the strength of the external magnetic field, or as one increases their mutual interaction by decreasing their separation, or by increasing their electric charge. A very similar picture emerges in the vortex-pair case. To

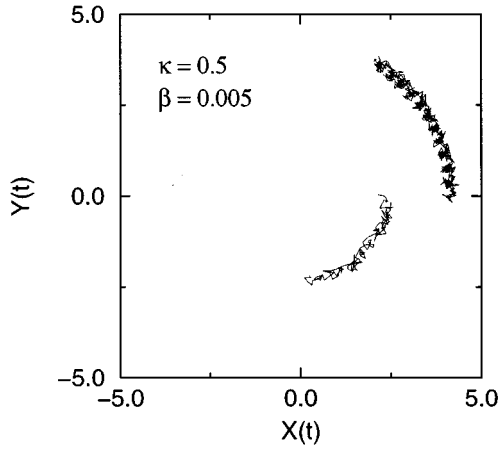


FIG. 9. In agreement to the theoretical prediction, when the $N = 1$ vortices attract each other, they rotate clockwise, while when they repel, they rotate counterclockwise.

study it we first performed a series of numerical experiments for various d 's, for the same values of the parameters $\kappa = 1.5$ and $\beta = 0.04$. The results depicted in Fig. 10, combined with Fig. 6, clearly confirm the claim that the cyclotron wavelength and width both decrease with the vortex-vortex force. Next, we varied β and followed the trajectory of the energy maximum corresponding to one of the two vortices for the same time interval in all cases. From the results shown in Fig. 11, it becomes apparent that an increase of β leads to a decrease of the corresponding cyclotron characteristics. Notice also from the same figure and Eq. (25), that the intervortex force increases with β .

So far we have dealt with small values of the parameter β , mainly in order to study the details of the cyclotron motion. As explained in Sec. II, though, a possible realistic set of parameters for a type-II superconductor is κ small and $\beta = 100$. Figure 12 depicts the result of the numerical inte-

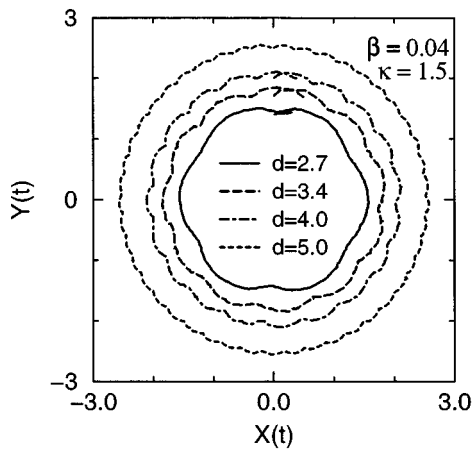


FIG. 10. The trajectory of the maximum of the energy density of one of the two vortices of the pair. The dependence of the characteristic wavelength and width of the cyclotron motion of each vortex on their separation d is qualitatively identical to the one obtained in the two-electron system.

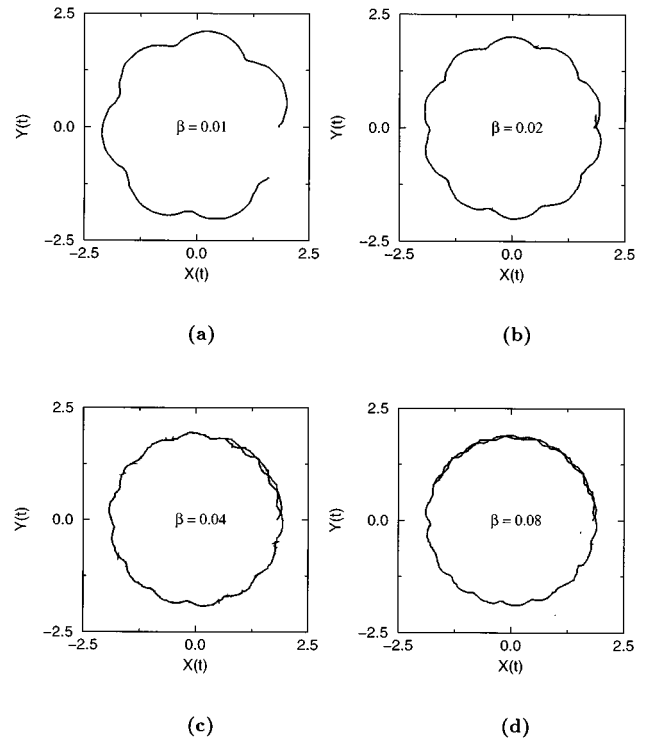


FIG. 11. The trajectory of the vortex, as determined from the position of the corresponding energy maximum, for various values of the parameter β and for the same total duration in all runs.

gration for an initial vortex-vortex separation $d = 3.5$. The cyclotron oscillations are now suppressed, the period has changed, but the vortices still move on a circle.

C. Vortex-antivortex system

We next replace one of the vortices of the pair by an $N = -1$ antivortex and let it evolve. Like in the analog electron-positron planar system with the external magnetic field and for reasonable initial velocities, we expect that, again up to a small cyclotron motion, the vortex and the

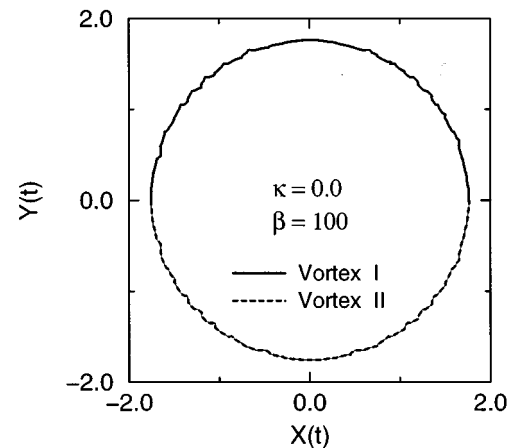


FIG. 12. The trajectories of the two vortices for half a period and for parameter values $\beta = 100$ and $\kappa = 0.0$.

antivortex will move in formation along parallel trajectories. This picture contradicts naive intuition, according to which the vortex and the antivortex would as a result of their attraction approach each other and gradually annihilate into elementary excitations.

A series of numerical experiments was performed with the vortex-antivortex system. The initial field configuration used was the product superposition of an $N=1$ and an $N=-1$ axially symmetric vortex solutions, according to the ansatz

$$\Psi(\mathbf{x}) = \Psi^{(1)}\left(\left|\mathbf{x} - \frac{\mathbf{d}}{2}\right|\right) \Psi^{(-1)}\left(\left|\mathbf{x} + \frac{\mathbf{d}}{2}\right|\right),$$

$$\mathbf{A}(\mathbf{x}) = \mathbf{A}^{(1)}\left(\left|\mathbf{x} - \frac{\mathbf{d}}{2}\right|\right) + \mathbf{A}^{(-1)}\left(\left|\mathbf{x} + \frac{\mathbf{d}}{2}\right|\right), \quad (34)$$

where $\Psi^{(1)}$ and $\mathbf{A}^{(1)}$ are the static fields of the $N=1$ vortex and $\Psi^{(-1)}$ and $\mathbf{A}^{(-1)}$ are those of the $N=-1$ antivortex. Like in the vortex-vortex case, A_0 is set to zero and the initial values of the electric field are obtained by solving Gauss' equation with the above Ψ .

The trajectories of the vortex and the antivortex in a typical run are illustrated in Fig. 13. Both the approximate guiding centers and the local maxima of the energy density were followed and are shown on the same plot. The parameters were set to $\kappa=1.5$ and $\beta=0.04$, while the initial positions of the vortex and the antivortex (zeros of the scalar field) were taken at $(-2,10)$ and $(2,10)$, respectively. The vortices moved in the negative y direction for 20 space units, i.e., about 16 times their size, while retaining their initial shape and keeping their initial separation constant. They moved with constant speed $V=0.025$. The vortex velocity in the vortex-vortex pair for the same values of parameters and separation was found to be $V=0.016$. The higher velocity in

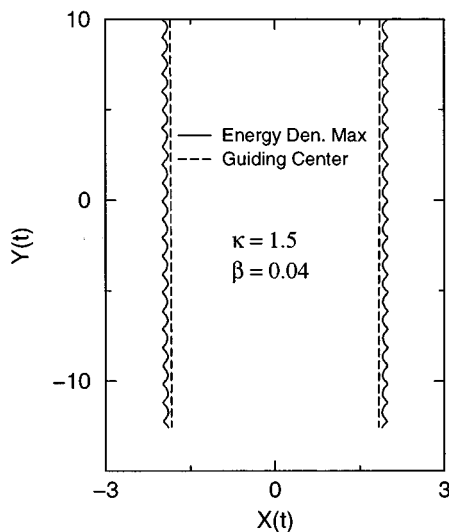


FIG. 13. The evolution of a typical initial vortex-antivortex configuration. The wavy and the straight lines are the trajectories of the energy density maxima and of the approximate guiding centers, respectively.

the vortex-antivortex case implies a potential between them steeper in absolute value than the one in Fig. 6.

Apart from the parallel transport of vortices, one sees a finer oscillating motion, the ‘‘cyclotron motion’’ we mentioned in the preceding paragraphs. We performed several runs to study its details for various values of d and β . As in the vortex pair system, both wavelength and width of the oscillation are decreasing functions of d and β , in perfect qualitative agreement with the dependence of the cycloid patterns in the electron-positron analogue.

We would like to end the discussion of the results with a final comment about boundary effects. As follows from Fig. 13, if we neglect the cyclotron motion, the paths of the two vortices are perfect straight lines parallel to the y axis. A slight convergence of the trajectories towards each other appears, though, when the vortices come close to the boundaries. Actually, if they start 6–7 space units away from the boundaries, the initial convergence disappears, to appear again when the vortices get close to the negative- y boundary. By trying different sizes of grids, one concludes that this behavior is a boundary effect sensitive to the absolute separation between the vortices and the boundaries, but insensitive to the size of the grid. In the case of relatively small grids, the convergence of the paths could be misleadingly interpreted as a generic feature of vortex dynamics. To avoid this effect in our numerical experiments we always placed the vortices sufficiently away from the boundaries of the grid.

V. DISCUSSION

The direct numerical integration of the motion of a generic vortex-(anti)vortex configuration confirms the Hall behavior, predicted analytically in a previous publication. The quantitative agreement persists even when the two solitons overlap to the point that they can hardly be considered as two. Physically, this behavior may not be entirely surprising. It might be described as the well-known Hall effect. After all the vortex of the model is microscopically¹⁶ a nonvanishing electric charge density, which is sustained by the nonlinear forces (attractive electrostatic and Ψ self-interactions) of the model, to circulate around its center, thus giving rise to the vortex magnetic field. The current is locally perpendicular to the electric field and hence consistent with the absence of energy dissipation. Thus, the overall situation looks similar to the ordinary Hall setting; only the circulating charges are immersed in their own magnetic field and repelled by it, instead of being kept in orbit by an externally prescribed one and, quite naturally, a vortex is expected to exhibit the Hall behavior described here. One may push the picture even further by noticing that since the charges as described by the wave function Ψ , are spread over the entire region of the vortex, and they feel the integral of the magnetic field, i.e., the winding number of the configuration, which makes plausible the appearance of N in formulas (24) and (23).

Mathematically, on the other hand, one is dealing with the most general model describing the dynamics of a condensate wave function Ψ coupled to the electromagnetic potential, and restricted only by the translational, rotational, and gauge invariance of the system. The ion lattice assumed frozen, defines a preferred reference frame, and breaks the Poin-

caré invariance of the underlying fundamental system. Topological or metastable nontopological solitons²¹ in models with just these symmetries²² are expected¹⁶ to exhibit identical Hall behavior. This is indeed what happens in all the systems examined so far,^{23,24} even in ferromagnets which have no physical similarity to a system of charges interacting with the electromagnetic field.^{11,25}

Clearly, the next step is to test the predictions of the model at hand against more realistic experimental situations. One should study the static properties of vortices in thin films with finite thickness, and then analyze their response to an external current in the context possibly of an improved model to incorporate dissipation.

ACKNOWLEDGMENTS

We would like to thank Professor N. Papanicolaou for several helpful discussions. G.N.S. would like to thank the University of Durham, where part of this work was performed, for its hospitality. This research was supported in part by the EU Grant Nos. CHRX-CT94-0621 and CHRX-CT93-0340, by the Greek General Secretariat of Research and Technology Grant No. 91ΠENEΔ358, and by a research fund from the University of Crete.

APPENDIX: THE NUMERICAL ALGORITHM

To solve the initial value problem defined by the system of equations (31) and a starting configuration of the form (33) or (34) we considered in this paper, we used a leapfrog updating scheme²⁶ where the time levels in the time derivative term “leapfrog” over the time levels in the space derivative term. Equations (31) are a mixed system of first-order and second-order differential equations in time. A leapfrog algorithm for a second-order equation is equivalent to the updating of fields and momenta successively, but the coupling of that equation to a first-order equation demands special care in the construction of the algorithm. Nevertheless, the leapfrog algorithm gives marked improvement in stability over the simpler approach of updating both fields and their momenta at the same time level.

To achieve sufficient accuracy in our computations we used a 161×161 grid, with lattice spacing $a=0.15$. The space resolution of that grid is estimated by calculating numerically the total topological charge N of Eq. (33) and comparing it to the exact value $N=2$. Using formula (19) for the topological charge one finds $N=1.993$. Interestingly, the alternative formula for $N=(1/2\pi)\int d^2x B$ is less sensitive to the discretization and gives $N=1.999$ for the initial configuration. The accuracy of our results is further estimated by the

conservation of the energy, which in all our runs remained constant to a degree better than 0.1% over a full period. We imposed Neumann boundary conditions by setting, the covariant derivative in the normal to the boundary direction, equal to zero. To do so we fixed the value of the Higgs field at each point of the external layer of the grid equal to their first inner neighbour. Also the values of the gauge fields, which live at the links which connect those neighbors, were set equal to zero. To test our results we repeated our runs on larger grids 251×251 with the same or smaller lattice spacing, say, $a=0.1$, and the results obtained were all perfectly consistent. We used a larger grid 251×251 and $a=0.15$ in the vortex-antivortex experiments in order to follow the orbits of the solitons for longer distances. The time step Δt we used in most of our runs was 0.001 or 0.002 but the algorithm was stable and accurate for even larger time steps. All our studies were performed on various HP workstations in Crete. A typical run of duration $T \approx 800$ time units, with $\Delta t=0.002$ on a 161×161 grid, needed about 80 hours of CPU time on a HP-735 machine.

Finally we wish to comment on our choice to use the formalism developed in the study of lattice gauge theories. One may envisage two discretization schemes to convert the equations of motion of our theory into difference equations: the conventional discretization scheme (CDS) and the lattice gauge formalism (LGF). We experimented with both and finally adopted the latter for its elegance and functionality. It should be pointed out that both methods have been used in the study of vortex dynamics in relativistic models,^{19,27-30} with satisfactory and consistent results. The LGF, especially designed to preserve the local constraint, is certainly more natural to use in a gauge theory, but for our problem there was another more serious issue to face. Use of any CDS explicitly violates gauge invariance. Without the gauge invariance there is no reason for the local constraint to be satisfied. In fact, a violation of the equation of continuity and of Gauss’ law was obtained, which in addition was accumulative in the runs based on any CDS we tried. Whenever the error in those became significant, the integration routine destabilized. The way out in the context of a CDS would be to use a sufficiently small time grid spacing to retain the error at sufficiently small values all during the time interval required for the study of the phenomenon of interest. This has worked reasonably well in the study of vortex scattering in relativistic models,^{27,28} since the process takes very little time and one is able to see the phenomenon on the computer without an excessive consumption of CPU time. In our case though this did not work. The vortices rotate very slowly around each other and in order to see a full turn one has to wait for a long time. In fact for a much too long time for any CDS we tried to be stable.

*Electronic address: stratos@physics.uch.gr

†Electronic address: tomaras@physics.uch.gr

¹R.P. Huebener, *Magnetic Flux Structures in Superconductors* (Springer-Verlag, Berlin, 1979).

²G. Blatter *et al.*, *Rev. Mod. Phys.* **66**, 1125 (1994).

³Ping Ao, *J. Supercond.* **8**, 1 (1995); S.J. Hagen *et al.*, *Phys. Rev. B* **41**, 11 630 (1990); V. Ambegaokar *et al.*, *ibid.* **21**, 1906

(1980); P. Nozières and W. Vinen, *Philos. Mag.* **14**, 667 (1966); J. Bardeen and M. Stephen, *Phys. Rev.* **140**, A1197 (1965).

⁴M.V. Feigel’man, V.B. Geshkenbeim, A.I. Larkin, and S. Levit, *JETP Lett.* **57**, 711 (1993); P. Ao and D.J. Thouless, *Phys. Rev. Lett* **70**, 2158 (1993); E. Šimánek, *Phys. Rev. B* **52**, 10 336 (1995).

⁵See, for instance, S.J. Hagen *et al.*, *Phys. Rev. B* **43**, 6246 (1991);

- H. van Beelen *et al.*, *Physica* **36**, 241 (1967); N. Usui *et al.*, *Phys. Lett.* **27A**, 140 (1968).
- ⁶A. Dorsey, *Phys. Rev. B* **46**, 8376 (1992).
- ⁷Qiang Li, J.R. Clem, and D.K. Finnemore, *Phys. Rev. B* **43**, 12 843 (1991).
- ⁸A. Schmid, *Phys. Kondens. Mater.* **5**, 302 (1966).
- ⁹L.P. Gor'kov and G.M. Éliashberg, *Sov. Phys. JETP* **27**, 328 (1968); L. Kramer and R.J. Watts-Tobin, *Phys. Rev. Lett.* **40**, 1041 (1978); G. Schön and V. Ambegaokar, *Phys. Rev. B* **19**, 3515 (1979); R.J. Watts-Tobin, Y. Krähelbühl, and L. Kramer, *J. Low Temp. Phys.* **42**, 459 (1981).
- ¹⁰A.P. Malozemoff and J.C. Slonczewski, *Magnetic Domain Walls in Bubble Materials* (Academic Press, New York, 1979).
- ¹¹N. Papanicolaou and T.N. Tomaras, *Nucl. Phys.* **B360**, 425 (1991).
- ¹²N. Papanicolaou and T.N. Tomaras, *Phys. Lett.* **179A**, 33 (1993).
- ¹³R.P. Feynman, *Statistical Mechanics*, *Frontiers in Physics* (Benjamin, New York, 1972).
- ¹⁴I.J.R. Aitchison *et al.* (unpublished); Ping Ao, D.J. Thouless, and X.-M. Zhu (unpublished); M. Stone (unpublished).
- ¹⁵A.A. Abrikosov, *Sov. Phys. JETP* **5**, 1174 (1957). For their counterparts in the relativistic Abelian-Higgs model, see H.B. Nielsen and P. Olesen, *Nucl. Phys.* **B61**, 45 (1973).
- ¹⁶G.N. Stratopoulos and T.N. Tomaras, *Physica D* **89**, 136 (1995).
- ¹⁷G.N. Stratopoulos, Ph.D. thesis, Department of Physics, University of Crete, 1996.
- ¹⁸Y. Aharonov, A. Casher, S. Coleman, and S. Nussinov, *Phys. Rev. D* **46**, 1877 (1992).
- ¹⁹M. Creutz, L. Jacobs, and C. Rebbi, *Phys. Rep.* **95**, 201 (1983).
- ²⁰D. Apostolakis, E. Floratos, and N. Vlachos (unpublished).
- ²¹C. Bachas and T. N. Tomaras, *Phys. Rev. D* **51**, R5356 (1995).
- ²²K. Lee, *Phys. Rev. D* **49**, 4265 (1994); I.V. Barashenkov and A.O. Harin, *ibid.* **52**, 2471 (1995).
- ²³X. G. Wen and A. Zee, *Phys. Rev. Lett.* **62**, 2873 (1989).
- ²⁴P. Donatis and R. Iengo (unpublished).
- ²⁵N. Papanicolaou and W. Zakrzewski, *Phys. Lett. A* **210**, 328 (1995); also *Physica D* **80**, 225 (1995).
- ²⁶W.H. Press, S.A. Teukolsky, W.T. Vetterling, and B.P. Flannery, *Numerical Recipes in Fortran* (Cambridge University Press, Cambridge, England, 1992).
- ²⁷E.P.S. Shellard and P.J. Ruback, *Phys. Lett.* **B209**, 262 (1988).
- ²⁸P. Laguna and R.A. Matzner, *Phys. Rev. D* **41**, 1751 (1990).
- ²⁹K.J.M. Moriarty, E. Myers, and C. Rebbi, *Comput. Phys. Commun.* **54**, 273 (1989).
- ³⁰E. Myers, C. Rebbi, and R. Strilka, *Phys. Rev. D* **45**, 1355 (1992).